Strong Localization of Majorana End States in Chains of Magnetic Adatoms

Yang Peng,[1] Falko Pientka,[1] Leonid I. Glazman,[2] and Felix von Oppen[1]
[1]Dahlem Center for Complex Quantum Systems and Fachbereich Physik, Freie Universität Berlin, 14195 Berlin, Germany
[2]Department of Physics, Yale University, New Haven, Connecticut 06520, USA
(Received 10 December 2014; published 9 March 2015)

A recent experiment [Nadj-Perge *et al*, Science 346, 602 (2014)] gives possible evidence for Majorana bound states in chains of magnetic adatoms placed on a superconductor. While many features of the observed end states are naturally interpreted in terms of Majorana states, their strong localization remained puzzling. We consider a linear chain of Anderson impurities on a superconductor as a minimal model and treat it largely analytically within mean-field theory. We explore the phase diagram, the subgap excitation spectrum, and the Majorana wave functions. Owing to a strong velocity renormalization, the latter are localized on a scale which is parametrically small compared to the coherence length of the host superconductor.

DOI: 10.1103/PhysRevLett.114.106801 PACS numbers: 73.63.Nm, 74.20.-z, 75.70.Tj, 75.75.-c

Introduction.—There is currently great interest in Majorana bound states in condensed-matter systems which realize non-Abelian quantum statistics [1,2] and which may have applications in topological quantum information processing [3]. Several platforms allow one to engineer topological superconducting phases supporting Majorana bound states, based on proximity coupling to s-wave superconductors (SCs). These include topological insulators [4,5], semiconductor quantum wires [6–8], and chains of magnetic adatoms [9–14] (see also Refs. [15–17]). All of these proposals are being actively pursued in the laboratory [18–26].

A recent experiment [26] exhibits signatures of Majorana bound states in chains of Fe atoms placed on a Pb surface. The experiment suggests that the Fe chain orders ferromagnetically. The subgap spectrum is probed by scanning tunneling spectroscopy with both spatial and spectral resolution, which shows zero-energy states near the ends of the chains. It is tempting to interpret these as Majorana bound states [26,27], as the system combines the three essential ingredients: (i) Proximity-induced superconductivity, (ii) a finite Zeeman splitting due to the exchange field of the ferromagnetic Fe chains, and (iii) Rashba spin-orbit (SO) coupling (presumably from the surface of the Pb substrate).

However, the observed localization of the end states on the scale of a few adatom sites is puzzling [28,29]. The Majorana localization length is typically estimated as $\xi_M = \hbar v_F/\Delta_{\rm top}$, while the coherence length ξ_0 of the proximity-providing SC is given by $\xi_0 = \hbar v_F/\Delta$. Here, we assume comparable Fermi velocities v_F in the one-dimensional electron system ("wire") and the host SC. At the same time, the induced topological gap $\Delta_{\rm top}$ is smaller than the host gap Δ. Thus, one may expect $\xi_M \gtrsim \xi_0$. This contrasts with the observation that the localization length of the end states is orders of magnitude smaller than the coherence length of Pb. Here we address this puzzle by modeling the adatoms as a chain of Anderson impurities hybridized with a SC and show that it predicts Majorana localization lengths which are parametrically smaller than ξ_0 over wide regions of parameter space.

The physics underlying the topological phase in chains of magnetic adatoms has been discussed using two approaches. One approach [9,10,30–33] starts with the subgap Shiba states [34–37] induced by the individual magnetic adatoms. The adatom is described as a classical magnetic moment which is exchange coupled to the electrons in the substrate, but otherwise electronically inert. Such Shiba chains exhibit topological superconducting phases and hence Majorana end states. An alternative approach [26,27] starts with exchange-split adatom states. While they are far from the Fermi energy for individual adatoms, hopping between the adatoms of the chain broadens these states into bands. For sufficiently strong hopping, these bands cross the Fermi energy and effectively realize a one-dimensional spin-polarized electron system. In this band limit, topological superconductivity is induced by proximity, in combination with SO coupling for ferromagnetic chains or helical magnetic order along the chain. As an additional benefit, our model unifies both of these approaches.

Heuristic considerations.—We start by discussing conventional proximity coupling of a free-electron wire to a bulk s-wave SC. The wire electrons are described by their Green function $G(k,E) = [E - v_F k\tau_z - \Sigma(k,E)]^{-1}$, where τ_i denote Pauli matrices in particle-hole space. The self-energy Σ accounts for the coupling to the SC and takes the familiar form [38,39]

$$\Sigma(k,E) = -\Gamma\frac{E+\Delta\tau_x}{\sqrt{\Delta^2-E^2}}. \quad (1)$$

Here, Γ measures the strength of hybridization between wire and SC. Far above the gap, $E \gg \Delta$, the SC behaves as a normal metal and the escape of electrons into the bulk SC is described by $\Sigma \simeq i\Gamma$. For subgap energies, electrons enter the SC only virtually and Σ becomes real.

For definiteness, consider energies far below the bulk gap, $E \ll \Delta$. Then, we can approximate $\Sigma \simeq -(\Gamma/\Delta)E - \Gamma\tau_x$, and $G(k,E) \simeq Z[E - Zv_F k\tau_z - Z\Gamma\tau_x]^{-1}$ with a renormalized quasiparticle weight $Z = [1+\Gamma/\Delta]^{-1}$, which describes the shift of the electrons' spectral weight from the wire into the SC. The quasiparticle weight ensures [1] that the induced s-wave gap (described by the pairing term $\propto \tau_x$) interpolates between the hybridization strength Γ at weak hybridization, $\Gamma \ll \Delta$, and the host gap Δ at strong hybridization, $\Gamma \gg \Delta$. It also renormalizes the Fermi velocity $v_F \to \tilde{v}_F = Zv_F$ which controls the coherence length of the induced superconductivity in the wire. Physically, the fraction of time an excitation spends in the wire is suppressed by Z, which reduces the effective velocity to Zv_F.

In adatom chains, the SO coupling in the SC allows for an induced p-wave pairing while the strong on-site repulsion and resulting spin polarization suppress s-wave correlations. Thus, the induced gap $\Delta_{\text{top}} = \alpha\Delta$ is now p wave and controlled by the (dimensionless) SO strength α. At the same time, it is natural to assume that the hybridization Γ modifies *single-particle* properties as before and the renormalization of v_F remains operative. This predicts a Majorana localization length

$$\xi_M = \hbar\tilde{v}_F/\Delta_{\text{top}} = Z\hbar v_F/\Delta_{\text{top}}. \tag{2}$$

For Fe adatoms in Pb, the hybridization is controlled by atomic scales so that $\Gamma \sim 1$ eV [26]. When compared to the host gap $\Delta \sim 10$ K, we find $Z \sim 10^{-3}$. This can dramatically suppress ξ_M relative to the host coherence length $\xi_0 \sim \hbar v_F/\Delta$ ($\simeq$100 nm for Pb). In fact, $\xi_M \sim \xi_0(\Delta/\Gamma)(\Delta/\Delta_{\text{top}})$, so that for $\alpha = \Delta_{\text{top}}/\Delta \sim 0.1$, the Majorana localization length ξ_M becomes of the order of the spacing between adatoms, as observed in Ref. [26].

Model.—We now show that these heuristic arguments are borne out in a microsopic model. We model the system as a linear chain of Anderson impurities placed in an s-wave SC. Each adatom hosts a spin-degenerate level of energy ϵ_d with on-site Hubbard repulsion U, representing the Fe d levels. We include nearest-neighbor hopping of strength w between these d levels as well as hybridization of strength t between the d levels and the SC. The model Hamiltonian

$$\mathcal{H} = \mathcal{H}_d + \mathcal{H}_s + \mathcal{H}_T \tag{3}$$

contains the BCS Hamiltonian $\mathcal{H}_s$ of the SC [40], the chain of d levels

$$\mathcal{H}_d = \sum_{j,\sigma}(\epsilon_d - \mu)d^\dagger_{j,\sigma}d_{j,\sigma} + U\sum_j n^\dagger_{j\uparrow}n_{j\downarrow} - w\sum_{j,\sigma}[d^\dagger_{j+1,\sigma}d_{j,\sigma} + d^\dagger_{j,\sigma}d_{j+1,\sigma}], \tag{4}$$

and their hybridization with the SC,

$$\mathcal{H}_T = -t\sum_{j,\sigma}[\psi^\dagger_\sigma(\mathbf{R}_j)d_{j,\sigma} + d^\dagger_{j,\sigma}\psi_\sigma(\mathbf{R}_j)]. \tag{5}$$

Here, $d_{j,\sigma}$ annihilates a spin-σ electron in the d level at site $\mathbf{R}_j = ja\hat{\mathbf{x}}$ of the chain, $n_{j,\sigma} = d^\dagger_{j,\sigma}d_{j,\sigma}$, and $\psi_\sigma(\mathbf{r})$ annihilates electrons at position $\mathbf{r}$ (taken as continuous) in the SC.

The model in Eq. (3) generalizes the Shiba chain model considered in Refs. [9,10]. It reduces to the Shiba chain in the limit of negligible spin fluctuations and weak intersite hopping w. Here, we include the hopping and the ensuing electronic dynamics of the magnetic adatoms within a mean-field treatment of the Hubbard term [41,42],

$$Un^\dagger_{j\uparrow}n_{j\downarrow} \to \frac{U}{2}\sum_\sigma[\langle n_j\rangle n_{j,\sigma} + \langle m_j\rangle\sigma n_{j,\sigma}], \tag{6}$$

where we defined the occupation $n_j = \sum_\sigma n_{j,\sigma}$ and the site polarization $m_j = n_{j,\uparrow} - n_{j,\downarrow}$. The first term merely renormalizes ϵ_d and will be absorbed in the following. The second term introduces a local exchange coupling in the adatom orbitals.

As we are predominantly interested in the localization of the Majorana modes, we do not aim at a self-consistent solution of the mean-field theory. Instead, we accept the formation of a spontaneous moment as experimental fact and explore its consequences. In the experiment, the moments order ferromagnetically along the chain. In this case, topological superconductivity requires Rashba SO coupling in the substrate SC [26,27,43,44]. For analytical tractability, we assume instead that the moments develop helical order $\mathbf{S}_j = (\sin\theta\cos\phi_j, \sin\theta\sin\phi_j, \cos\theta)$ with $\phi_j = 2k_h ja$ and $\theta = \pi/2$. We emphasize that the model with helical order can be mapped to a ferromagnetic model with SO coupling in both the adatom d band and the substrate SC. Strictly speaking, the substrate SO coupling generated by the mapping differs from conventional Rashba coupling, but it does include the specific term that allows for proximity-induced p-wave pairing. The mapping is effected by the unitary transformation $d_j \to e^{-ik_h ja\sigma_z}d_j$ and $\psi(\mathbf{r}) \to e^{-ik_h x\sigma_z}\psi(\mathbf{r})$, which rotates the spin basis along the direction of the local impurity moments [45,46].

Excitation spectrum and phase diagram.—In mean-field theory, we can describe the system equivalently by the corresponding Bogoliubov–de Gennes Hamiltonian $H = H_d + H_s + H_T$ (after the above-mentioned unitary transformation) and consider the Green function $G = (E-H)^{-1}$. In view of the local nature of the hybridization H_T, we can write a closed set of equations for the restricted Green function $g_{ij} = G(\mathbf{R}_i, \mathbf{R}_j)$ defined at the sites of the adatoms,

$$\begin{pmatrix} (g_0^{\text{ss}})^{-1} & t\tau_z \\ t\tau_z & E - H_d \end{pmatrix} g = 1. \tag{7}$$

We use the Pauli matrices τ_i (σ_i) in particle-hole (spin) space. The bare Green function of the SC restricted to the adatom sites and subgap energies is readily obtained within BCS theory (see Ref. [46] for more details),

$$g^{\rm ss}_{0,ij}(E) = -\pi\nu_0 \exp(-ik_h x_{ij}\sigma_z) \times \left\{ \frac{E+\Delta\tau_x}{\sqrt{\Delta^2-E^2}} {\rm Im} f(r_{ij}) + \tau_z {\rm Re} f(r_{ij}) \right\}, \quad (8)$$

where ν_0 is the normal density of state at the Fermi level, $f(r) = e^{ik_F r - r/\xi_E}/k_F r$, and $\xi_E = \hbar v_F/\sqrt{\Delta^2 - E^2}$. Equation (8) is valid for $i \neq j$, but also applies to $i = j$ when dropping the Ref term. Here, the factor $\exp(-ik_h x_{ij}\sigma_z)$ is induced by the unitary transformation.

The subgap excitation spectrum may then be obtained from the poles of $g^{\rm ss} = g^{\rm ss}_0[1 - \Sigma g^{\rm ss}_0]^{-1}$ where we define the self-energy $\Sigma = t g^{\rm dd}_0 t = t(E - H_d)^{-1} t$. As $g^{\rm ss}_0$ has no poles at subgap energies, this yields the condition $\det[1 - \Sigma g^{\rm ss}_0] = 0$. In (lattice) momentum representation, the determinant involves a 4×4 matrix with [46]

$$g^{\rm ss}_0(k,E) = \pi\nu_0 \left\{ \frac{E+\Delta\tau_x}{\sqrt{\Delta^2-E^2}} L_i^{\sigma_z}(k,E) + \tau_z L_r^{\sigma_z}(k,E) \right\}. \quad (9)$$

Here, $L_r^{\sigma_z}$ and $L_i^{\sigma_z}$ are real and imaginary parts of the function $L^{\sigma_z} = F(k + k_h\sigma_z) - i$, respectively, with $F(k) = (1/k_F a)\ln\{1 - e^{i(k_F+k)a - a/\xi_E}\} + (k \leftrightarrow -k)$ [48]. Computing the dispersions and identifying phase boundaries by the closing of the gap, we first obtain representative phase diagrams of the adatom chain, as shown in Fig. 1.

These phase diagrams plot the topological (BDI [49]) index and make the interpolation between the band and Shiba limits explicit. The Shiba limit corresponds to weak hopping w between d levels. Here, topological superconductivity requires deep Shiba states so that the Shiba bands cross the chemical potential at the center of the host gap [10]. The band limit corresponds to weak hybridization $\Gamma = \pi\nu_0 t^2$ and thus Shiba states with energies E_s near Δ [42,46]. Then, topological superconductivity requires that one spin-polarized d band crosses the Fermi energy. The range over which this happens depends on the asymmetry of the bare exchange-split adatom states $E_{d,\sigma} = \epsilon_d - \sigma U\langle m\rangle/2$ around the chemical potential (set to $\mu = 0$). Figure 1(a) shows the symmetric case $E_{d,\uparrow} = -E_{d,\downarrow}$. There is only a narrow topological interval in w for small Γ ($E_s \simeq \Delta$) because despite the large exchange splitting of the d levels, the spin-split d bands cross μ at the same hopping strength w. As the asymmetry between $E_{d,\uparrow}$ and $E_{d,\downarrow}$ around μ increases, the d bands cross μ at different values of w, and the adatom states are perfectly spin polarized at the chemical potential over a substantial region in w; cf. Fig. 1(b).

For fully analytical results, we consider the limit of strong asymmetry with $E_{d,\uparrow} \to -\infty$ at a fixed $E_{d,\downarrow}$. In this limit, only the spin-down band $E_d = E_{d,\downarrow} - w\sum_{\pm}\cos(k \pm k_h)a$ of the d levels is relevant. A detailed but straightforward calculation [46] now shows that the condition $\det(1 - \Sigma g^{\rm ss}_0) = 0$ can be reduced to the determinant of a 2×2 matrix and written in the form

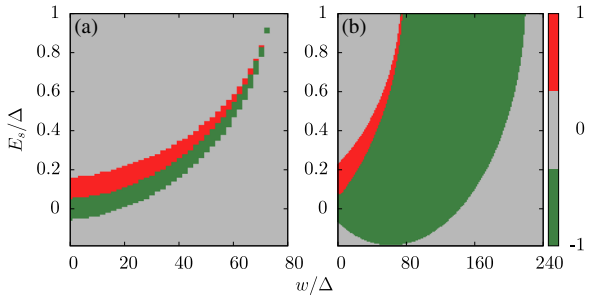

FIG. 1 (color online). Representative phase diagrams for the adatom chain as a function of the Shiba state energy E_s of an individual impurity and the hopping amplitude w between d levels. The colors indicate the topological index (grey: topologically trivial; red or green: topological phase with index ± 1). We chose $E_{d,\downarrow} = 100\Delta$, $k_F a = 4.3\pi$, $k_h a = 0.26\pi$, and $\xi_0/a = \infty$. The panels correspond to (a) symmetric adatom d bands ($E_{d,\uparrow} = -100\Delta$) and (b) asymmetric adatom d bands ($E_{d,\uparrow} = -300\Delta$). Here, $E_{d,\sigma} = \epsilon_d - \sigma U\langle m\rangle/2$.

$$(\Delta^2 - E^2)[E_d + \Gamma L_r]^2 - E^2[\sqrt{\Delta^2 - E^2} - \Gamma L_i]^2 + \Gamma^2\Delta^2(\delta L_i)^2 = 0. \quad (10)$$

Here, we introduced the shorthand notations $L_{r/i} = (L^+_{r/i} + L^-_{r,i})/2$ and $\delta L_i = (L^+_i - L^-_i)/2$. Equation (10) is an implicit equation for the subgap excitation spectrum E_k of the adatom chain in the strongly asymmetric limit. [Note that we have suppressed all k labels in Eq. (10).]

In the limits $\Gamma \ll \Delta$ and $\Gamma \gg \Delta$, Eq. (10) gives explicit analytical expressions for the excitation spectrum throughout the entire Brillouin zone. These are obtained by keeping only the respective dominant term in the second square brackets on the left-hand side, in excellent agreement with the full Green-function solution in Figs. 2(a)–2(c). We note that there is a single subgap state for every lattice momentum k; i.e., there is one subgap state per adatom, as in the Shiba limit (small w).

Majorana wave function.—Equation (10) also encapsulates the localization of the Majorana wave functions. In the Shiba limit of small w, the Majorana localization was addressed previously [50]. Here, we focus on the band limit of large w where the spin-down d band E_d crosses the Fermi energy of the SC, as is presumably the case in the experiment [26,27]. E_d crosses $\mu = 0$ at momenta k_0, so that $E_d \simeq v_F(k - k_0)$, where v_F is the Fermi velocity of the d band at the chemical potential of the SC. Similarly, $E_d + \Gamma L_r \simeq v_F(k - k_0)$, where we simply absorb the parametrically small shifts in v_F and k_0 due to ΓL_r into their definitions.

The decay of the Majorana wave function is controlled by the behavior of the dispersion near the minimal gap at k_0. Assuming that the pitch of the spin helix (or, equivalently, the strength of SO coupling) is not too large, this topological gap will be small compared to the gap Δ of the superconducting host. Then, E is small compared to Δ in the relevant region and Eq. (10) simplifies significantly. Consider first the limit of weak hybridization $\Gamma \ll \Delta$. In this limit, Eq. (10) reduces to

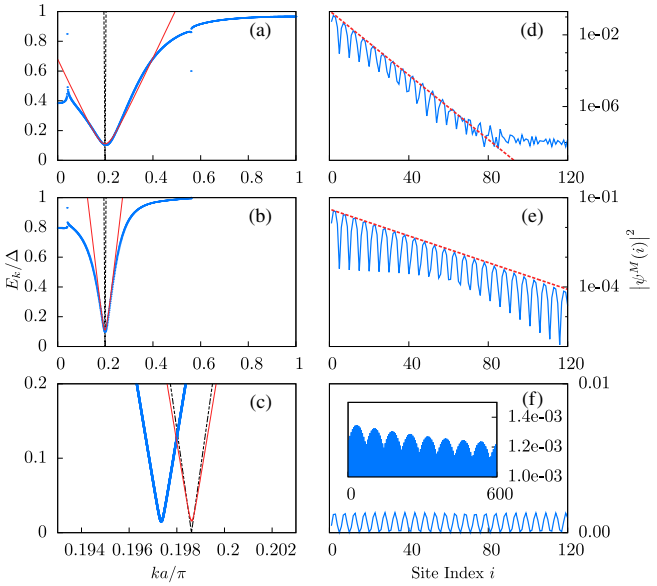

FIG. 2 (color online). Excitation spectra E_k for $ka/\pi \in [0,1]$ and (a) $\Gamma = 64\Delta$, (b) $\Gamma = 16\Delta$, and (c) $\Gamma = 0.16\Delta$. We choose $k_F a = 4.3\pi$, $k_h a = 0.26\pi$, $E_{d,\downarrow} = 100\Delta$, $E_{d,\uparrow} = -19900\Delta$, $w = 90\Delta$, and $\xi_0/a = \infty$. The dashed lines are subgap dispersions of the impurity chain without coupling to the SC. The blue curves are exact dispersions. The red curves are calculated using Eq. (12) for $\Gamma \gg \Delta$ and Eq. (11) for $\Gamma \ll \Delta$. Notice that the horizontal axis in (c) is restricted to a very narrow range and that the deviation between the red and blue curves is indeed small. Panels (d), (e), and (f) show Majorana wave functions $|\psi^M(i)|^2$ (blue lines) obtained for a finite chain of length $L = 1500a$. Only the first 120 sites i are shown. (d) and (e) are plotted on a logarithmic scale and the red dashed lines are fits using Eq. (2) for the Majorana localization length. (f) is plotted on a linear scale. (Inset) Decay over the first 600 sites.

$$E_k = \pm\sqrt{[v_F(k-k_0)]^2 + \Gamma^2(\delta L_i)^2}, \qquad (11)$$

where δL_i should be evaluated at k_0. We identify the topological gap $\Delta_{\text{top}} = \Gamma(\delta L_i)_{k=k_0}$, which is small compared to Δ. The Majorana wave function is expected to decay on the characteristic length scale of this dispersion; i.e., we find the Majorana localization length $\xi_M = \hbar v_F/\Delta_{\text{top}}$, consistent with the heuristic argument above for $\Gamma \ll \Delta$. For the numerical parameters of Fig. 2(c), ξ_M is larger than the length of the chain, making a direct comparison impossible.

The experiment is in the limit of the large hybridization $\Gamma \gg \Delta$, where Eq. (10) predicts a low-energy dispersion

$$E_k = \pm\sqrt{[(\Delta/\Gamma L_i)v_F(k-k_0)]^2 + [\Delta(\delta L_i/L_i)]^2}. \qquad (12)$$

In this limit, the induced gap $\Delta_{\text{top}} = \Delta(\delta L_i/L_i)_{k=k_0}$ is independent of Γ and saturates to a value which is smaller than Δ by a factor measuring the effective strength of the SO coupling. The strong hybridization with the SC also induces a dramatic downward renormalization of the Fermi velocity of the excitations, $v_F \to \tilde{v}_F = (\Delta/\Gamma L_i)v_F$. These

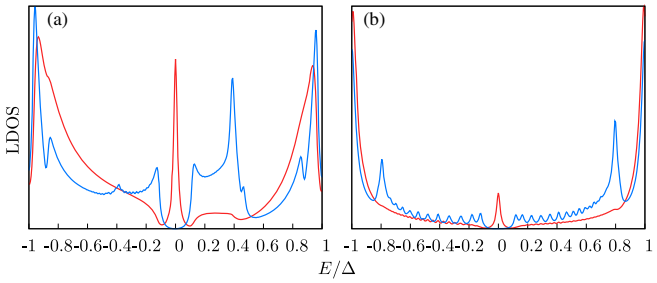

FIG. 3 (color online). Local density of states of particle excitations, computed in the center (blue lines) and at the end (red lines), for a chain of length $L = 300a$ and hybridizations (a) $\Gamma = 64\Delta$ and (b) $\Gamma = 16\Delta$. Other parameters are as in Fig. 2.

features are in excellent agreement with the numerical subgap spectra shown in Figs. 2(a) and 2(b) and vindicate our introductory heuristic arguments. Indeed, Eq. (12) predicts a Majorana localization length $\xi_M = \hbar v_F/(\Gamma\delta L_i)$, which coincides with Eq. (2) from heuristic consideration. We see that ξ_M is independent of the host gap Δ and controlled instead by the hybridization Γ. This result is in excellent agreement with numerical Majorana wave functions for $\Gamma \gg \Delta$; see Figs. 2(d) and 2(e).

The topological gaps in Eqs. (11) and (12) are both enabled explicitly by the SO coupling in the substrate which enters via the L factors in g_0^{ss}. In contrast, the SO coupling in the d band is fully ineffective due to the strong spin polarization. Parametrically, one finds $\delta L_i \simeq \delta L_i/L_i \simeq k_h/k_F$ in the limit $k_F a \gg 1$.

Notice that Eqs. (12) and (2) require the condition $\Gamma \ll v_F/a$. This condition ensures that the in-band propagation between adjacent sites, taking time $\tau \sim a/\tilde{v}_F$, is faster than hopping via the host SC, taking time $(\Delta L_r)^{-1}$ [10]. Then, the $k = k_0$ minimum described by Eq. (12) dominates over the additional features of the quasiparticle spectrum associated with logarithmic divergencies in L_r. They induce power-law tails in the Majorana wave functions [cf. Fig. 2(d)] which become correspondingly more pronounced as Γ increases.

Local density of states.—We have also numerically computed [46] the local density of states of the adatom chain; see Fig. 3. The zero-bias peak grows more pronounced with increasing Γ, reflecting the stronger localization of the Majorana wave function. In addition to the zero-energy Majorana peak, one discerns additional peaks at finite energies which arise from van Hove singularities in the subgap Shiba band and which approach the center of the gap as the hybridization Γ increases. The zero-energy features and their strong localization as well as the van Hove peaks are consistent with the experimental observations [26].

We thank Ali Yazdani, Andrei Bernevig, Titus Neupert, Piet Brouwer, and Allan MacDonald for the stimulating discussions. We acknowledge financial support from the Helmholtz Virtual Institute "New states of matter and their excitations," Grants No. SPP1285 and No. SPP1666 of the Deutsche Forschungsgemeinschaft, the Humboldt

Foundation, NSF DMR Grant No. 1206612, and ONR Grant No. Q00704. We are grateful to the Aspen Center for Physics, supported by NSF Grant No. PHYS-106629, for their hospitality while this line of work was initiated.

[1] J. Alicea, Rep. Prog. Phys. **75**, 076501 (2012).
[2] C. W. J. Beenakker, Annu. Rev. Condens. Matter Phys. **4**, 113 (2013).
[3] A. Kitaev, Ann. Phys. (Amsterdam) **303**, 2 (2003).
[4] L. Fu and C. L. Kane, Phys. Rev. Lett. **100**, 096407 (2008).
[5] L. Fu and C. L. Kane, Phys. Rev. B **79**, 161408(R) (2009).
[6] R. M. Lutchyn, J. D. Sau, and S. Das Sarma, Phys. Rev. Lett. **105**, 077001 (2010).
[7] Y. Oreg, G. Refael, and F. von Oppen, Phys. Rev. Lett. **105**, 177002 (2010).
[8] J. Alicea, Y. Oreg, G. Refael, F. von Oppen, and M. P. A. Fisher, Nat. Phys. **7**, 412 (2011).
[9] S. Nadj-Perge, I. K. Drozdov, B. A. Bernevig, and A. Yazdani, Phys. Rev. B **88**, 020407(R) (2013).
[10] F. Pientka, L. I. Glazman, and F. von Oppen, Phys. Rev. B **88**, 155420 (2013).
[11] Y. Kim, M. Cheng, B. Bauer, R. M. Lutchyn, and S. Das Sarma, Phys. Rev. B **90**, 060401(R) (2014).
[12] J. Klinovaja, P. Stano, A. Yazdani, and D. Loss, Phys. Rev. Lett. **111**, 186805 (2013).
[13] B. Braunecker and P. Simon, Phys. Rev. Lett. **111**, 147202 (2013).
[14] M. M. Vazifeh and M. Franz, Phys. Rev. Lett. **111**, 206802 (2013).
[15] T.-P. Choy, J. M. Edge, A. R. Akhmerov, and C. W. J. Beenakker, Phys. Rev. B **84**, 195442 (2011).
[16] M. Kjaergaard, K. Wölms, and K. Flensberg, Phys. Rev. B **85**, 020503 (2012).
[17] I. Martin and A. F. Morpurgo, Phys. Rev. B **85**, 144505 (2012).
[18] V. Mourik, K. Zuo, S. M. Frolov, S. R. Plissard, E. P. A. M. Bakkers, and L. P. Kouwenhoven, Science **336**, 1003 (2012).
[19] A. Das, Y. Ronen, Y. Most, Y. Oreg, M. Heiblum, and H. Shtrikman, Nat. Phys. **8**, 887 (2012).
[20] H. O. H. Churchill, V. Fatemi, K. Grove-Rasmussen, M. T. Deng, P. Caroff, H. Q. Xu, and C. M. Marcus, Phys. Rev. B **87**, 241401(R) (2013).
[21] L. P. Rokhinson, X. Liu, and J. K. Furdyna, Nat. Phys. **8**, 795 (2012).
[22] M. T. Deng, C. L. Yu, G. Y. Huang, M. Larsson, P. Caroff, and H. Q. Xu, Nano Lett. **12**, 6414 (2012).
[23] A. D. K. Finck, D. J. Van Harlingen, P. K. Mohseni, K. Jung, and X. Li, Phys. Rev. Lett. **110**, 126406 (2013).
[24] S. Hart, H. Ren, T. Wagner, P. Leubner, M. Mühlbauer, C. Brüne, H. Buhmann, L. W. Molenkamp, and A. Yacoby, Nat. Phys. **10**, 638 (2014).
[25] V. S. Pribiag, A. J. A. Beukman, F. Qu, M. C. Cassidy, C. Charpentier, W. Wegscheider, and L. P. Kouwenhoven, Edge-mode superconductivity in a two dimensional topological insulator, arXiv:1408.1701.
[26] S. Nadj-Perge, I. K. Drozdov, J. Li, H. Chen, S. Jeon, J. Seo, A. H. MacDonald, B. A. Bernevig, and A. Yazdani, Science **346**, 602 (2014).
[27] J. Li, H. Chen, I. K. Drozdov, A. Yazdani, B. A. Bernevig, and A. H. MacDonald, Phys. Rev. B **90**, 235433 (2014).
[28] E. Dumitrescu, B. Roberts, S. Tewari, J. D. Sau, and S. Das Sarma, Majorana fermions in chiral topological ferromagnetic nanowires, arXiv:1410.5412.
[29] P. A. Lee, commentary on Ref. [26], Journal Club for Condensed Matter Physics, http://www.condmatjournalclub.org/?m=201410.
[30] S. Nakosai, Y. Tanaka, and N. Nagaosa, Phys. Rev. B **88**, 180503(R) (2013).
[31] K. Pöyhönen, A. Westström, J. Röntynen, and T. Ojanen, Phys. Rev. B **89**, 115109 (2014).
[32] A. Heimes, P. Kotetes, and G. Schön, Phys. Rev. B **90**, 060507 (R) (2014); A. Heimes, D. Mendler, and P. Kotetes, Interplay of topological phases in magnetic adatom-chains on top of a Rashba superconducting surface, arXiv:1410.6367.
[33] P. M. R. Brydon, H. Y. Hui, and J. D. Sau, Topological Shiba chain from spin-orbit coupling, arXiv:1407.6345.
[34] L. Yu, Acta Phys. Sin. **21**, 75 (1965).
[35] H. Shiba, Prog. Theor. Phys. **40**, 435 (1968).
[36] A. I. Rusinov, Pis'ma Zh. Eksp. Teor. Fiz. **9**, 146 (1968) [JETP Lett. **9**, 85 (1969)].
[37] A. V. Balatsky, I. Vekhter, and J.-X. Zhu, Rev. Mod. Phys. **78**, 373 (2006).
[38] A. C. Potter and P. A. Lee, Phys. Rev. B **83**, 184520 (2011).
[39] A. A. Zyuzin, D. Rainis, J. Klinovaja, and D. Loss, Phys. Rev. Lett. **111**, 056802 (2013).
[40] We assume that the bulk gapΔ remains unaffected by the adatoms. While we expect that the renormalization of v_F as a single-particle quantity remains operative, studying self-consistent effects on Δ may be an interesting problem for future research [see I. Reis, D. J. J. Marchand, and M. Franz, Phys. Rev. B **90**, 085124 (2014)]; T. Meng, J. Klinovaja, S. Hoffman, P. Simon, and D. Loss, Superconducting gap renormalization around two magnetic impurities: From Shiba to Andreev bound states, arXiv:1501.07901.
[41] P. W. Anderson, Phys. Rev. **124**, 41 (1961).
[42] H. Shiba, Prog. Theor. Phys. **50**, 50 (1973).
[43] M. Duckheim and P. W. Brouwer, Phys. Rev. B **83**, 054513 (2011).
[44] S. B. Chung, H. J. Zhang, X. L. Qi, and S. C. Zhang, Phys. Rev. B **84**, 060510(R) (2011).
[45] B. Braunecker, G. I. Japaridze, J. Klinovaja, and D. Loss, Phys. Rev. B **82**, 045127 (2010).
[46] See Supplementary Material at http://link.aps.org/supplemental/10.1103/PhysRevLett.114.106801, which includes Ref. [47], for the unitary transformation of Hamiltonian of helical order, definition of the Shiba state energy, derivation of the lattice Green function, description of the numerics, derivation of Eq. (10) of main text and more discussions on the comparison with experiment.
[47] A. Fetter and D. Walecka, *Quantum Theory of Many Particle Systems* (McGraw-Hill, New York, 1971).
[48] The function L is plotted in Ref. [46]. Roughly, $L_i^{\sigma_z}$ (and hence L_i) is of order unity. $L_r^{\sigma_z}$ (and hence L_r) is of order $1/k_F a$, except at isolated values of k where it has logarithmic singularities. δL_i should be thought of as a dimensionless measure of the effective SO strength, which is also of order $1/k_F a$ for our spin-helix model.
[49] S. Ryu, A. P. Schnyder, A. Furusaki, and A. W. W. Ludwig, New J. Phys. **12**, 065010 (2010).
[50] F. Pientka, L. I. Glazman, and F. von Oppen, Phys. Rev. B **89**, 180505(R) (2014).